

Momentum-dependent sign-inversion of orbital polarization in superconducting FeSe

Y. Suzuki¹, T. Shimojima¹, T. Sonobe¹, A. Nakamura¹, M. Sakano¹, H. Tsuji¹,
J. Omachi², K. Yoshioka³, M. Kuwata-Gonokami^{2,3}, T. Watashige⁴, R. Kobayashi⁴, S. Kasahara⁴,
T. Shibauchi⁵, Y. Matsuda⁴, Y. Yamakawa⁶, H. Kontani⁶, K. Ishizaka¹

¹*Quantum-Phase Electronics Center (QPEC) and Department of Applied Physics, University of Tokyo, Bunkyo, Tokyo 113-8656, Japan*

²*Photon Science Center, The University of Tokyo, 7-3-1 Hongo, Bunkyo-ku, Tokyo 113-8656, Japan*

³*Department of Physics, The University of Tokyo, 7-3-1 Hongo, Bunkyo-ku, Tokyo 113-0033, Japan*

⁴*Department of Physics, Kyoto University, Kyoto 606-8502, Japan*

⁵*Department of Advanced Materials Science, University of Tokyo, Chiba 277-8561, Japan*

⁶*Department of Physics, Nagoya University, Furo-cho, Nagoya 464-8602, Japan*

We investigate the electronic reconstruction across the tetragonal-orthorhombic structural transition in FeSe by employing polarization-dependent angle-resolved photoemission spectroscopy (ARPES) on detwinned single crystals. Across the structural transition, the electronic structures around the Γ and M points are modified from four-fold to two-fold symmetry due to the lifting of degeneracy in d_{xz}/d_{yz} orbitals. The d_{xz} band shifts upward at the Γ point while it moves downward at the M point, suggesting that the electronic structure of orthorhombic FeSe is characterized by a momentum-dependent sign-changing orbital polarization. The elongated directions of the elliptical Fermi surfaces (FSs) at the Γ and M points are rotated by 90 degrees with respect to each other, which may be related to the absence of the antiferromagnetic order in FeSe.

Keywords:

PACS:

Most of the parent compounds of the iron-based superconductors show the tetragonal-orthorhombic structural transition at T_s and the stripe-type antiferromagnetic (AFM) order below T_N ($\leq T_s$) [1,2]. Near the structural transition, an orbital order defined by the inequivalent electron occupation of $3d_{xz}$ (xz) and $3d_{yz}$ (yz) orbitals [3-5], has been reported by ARPES [6,7] and X-ray linear dichroism measurements [8] in several parent compounds. Experimental and theoretical studies suggested that the structural transition is caused by the electronic nematicity of the spin [9,10] or orbital [11-13] degrees of freedoms. Since superconductivity develops when such complex ordered states are suppressed, it is crucial to understand how the phase transitions couple to each other.

In $\text{Ba}(\text{Fe},\text{Co})_2\text{As}_2$, the spin-driven nematicity has been suggested from the phase diagram in which T_s and T_N closely follow each other as the carrier is doped [14]. The scaling behavior between the nematic fluctuation and spin fluctuation was also reported by the nuclear magnetic resonance (NMR) and shear modulus measurements [10]. On the other hand, in NaFeAs , the orbital-driven nematicity has been proposed by ARPES [11]. In this compound, the structural transition at $T_s = 54$ K is well separated from the AFM transition at $T_N = 43$ K. Inequivalent shift in the xz/yz orbital bands appearing above T_s changes the FSs from four-fold to two-fold symmetric shape [11,15], which may be a possible trigger of the stripe type AFM order and the orthorhombicity [11,16]. The variety of iron-based

superconductors thus requires us to investigate how the driving force of the electronic nematicity depends on each material class.

FeSe is a good example to examine the role of orbital degrees of freedom, since it shows the structural and superconducting (SC) transitions at $T_s \sim 90$ K and $T_c = 9$ K without any magnetic order [17]. Recent ARPES studies on FeSe reported a lifting of degeneracy in xz/yz orbitals at the M point showing up at low temperature [12,18-21]. Since the difference in the energy between xz and yz bands is much larger than that expected from the orthorhombic lattice distortion alone, it is considered to be an indication of the electronic nematicity of orbital-origin [12]. It is further expected that the unconventional superconductivity with nodal superconducting gaps is realized in FeSe [22,23] on the two-fold FSs in the orbital ordered state. While a drastic modification of the FSs has been reported by ARPES on twinned crystals [19], there has been no report directly showing the two-fold symmetry of the FS shape and its orbital character in the single domain. In order to understand the orbital-driven nematicity and its relation to the superconductivity, we must clarify how the orbital order affects the electronic structure in the entire Brillouin zone (BZ) by using the detwinned crystals of FeSe.

In this Letter, we report the electronic reconstruction across T_s of FeSe by using He-discharge lamp and laser-ARPES on detwinned crystals.

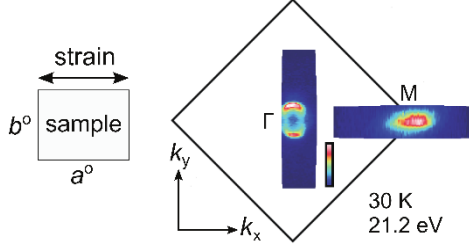


Figure 1. Fermi surface mapping taken at 30K by $h\nu = 21.2$ eV. Black square represents the tetragonal Brillouin zone. x and y are coordinates along the crystal axes of the orthorhombic setting a° and b° , respectively ($a^\circ > b^\circ$). The a° axis is aligned along the direction of the uniaxial tensile strain.

We observed a drastic modification of FSs from four-fold to two-fold symmetry around both the Γ and M points. The electron FS at the M point and the hole FS at the Γ point were found to be of elliptical shape rotated by 90 degrees with respect to each other. Polarization-dependent ARPES further revealed that the xz orbital shifts upward at the Γ point while it moves downward at the M point, thus indicating a momentum-dependent sign-inversion of orbital polarization in xz/yz orbitals. Imperfect FS nesting condition in the orthorhombic phase might be related to the absence of the antiferromagnetic order in FeSe.

High quality single crystals of FeSe were synthesized as described in ref.17. The transition temperatures of the single crystals were estimated to be $T_s \sim 90$ K and $T_c \sim 9$ K from the electrical resistivity measurements. For the FS mapping below T_s , we used a VG-Scienta R4000WAL electron analyzer and a helium discharge lamp of $h\nu = 21.2$ eV at the University of Tokyo. The energy resolution was set to 15 meV. For the polarization-dependent ARPES at the Γ point, we employed the fourth-harmonic generation of Ti:sapphire laser radiation ($h\nu = 5.9$ eV) [24] and a VG-Scienta R4000WAL electron analyzer at the University of Tokyo. We chose s and p polarizations to determine the orbital characters. The energy resolution was set to be 6 meV. To detwin the single crystals, we applied an in-plane uniaxial tensile strain, which brings the orthorhombic a° axis ($a^\circ > b^\circ$) along its direction below T_s (see Fig. 1). Samples were cleaved *in situ* at room temperature in an ultrahigh vacuum of 5×10^{-11} Torr.

Shown in Fig. 1 is the FS mapping with an energy window of ± 5 meV taken at 30 K ($T < T_s$) for detwinned FeSe. In the orthorhombic phase, we found one elliptical hole FS at Γ and one elliptical electron FS at M , with the long axes along k_y and k_x , respectively. According to our previous ARPES on detwinned FeSe [12], elliptical intensity at the M point is mainly derived from the electron bands composed of xz orbital along k_x and yz orbital along k_y direction. It is in a strong contrast to the high temperature tetragonal phase, where a small circular hole FS at Γ and two crossing elliptical electron FSs at M are observed in the four-fold symmetry [12].

In order to assign the orbital characters of the band dispersions which make the hole FS around the Γ point, we employed laser-ARPES with s - and p -polarizations. Considering the parity symmetry of light polarizations with respect to a mirror plane, one can assign the orbital character for each band dispersion [25]. In Figs. 2(a) and 2(b), we illustrate the experimental geometries for different sample orientations. In Geometry 1 where the strain direction is parallel to the detector slit, the momentum along the short axis of the elliptical FS is measured. Here, yz and xy (xz) orbitals have odd (even) symmetry with respect to the mirror plane and can be detected by s (p)-polarized light. In a similar way, xz and xy (yz) are supposed to be detected by s (p)-polarized light in Geometry 2 which measures along the long axis of the elliptical FS.

Figs. 2 (c-e) show an E - k image, its second E derivative image and the schematic band dispersion obtained by laser-ARPES in Geometry 1 (along k_x) at 160 K, respectively. The left and right panels are the results taken by s - and p -polarized light, respectively. In Figs. 2(c) and (d), one can find that the α band crosses E_F at the Fermi momentum (k_F) of $\sim 0.07 \text{ \AA}^{-1}$ while the top of the β band locates at $E - E_F \sim -10$ meV. In Geometry 2, α' and β' hole bands are similarly observed as shown in Figs. 2(f) and 2(g). Considering the polarization dependence in Geometries 1 and 2, α and β' (β and α') bands are consistently assigned to be dominantly of yz (xz) orbital character. Relatively flat band of low intensity around $E - E_F \sim -50$ meV only detected by s -polarization originates from xy orbital component. Schematic band structures in the tetragonal phase are then summarized in Fig. 2 (e and h). These results suggest that the circular hole FS around the Γ point is equally composed of xz and yz orbital characters.

ARPES images taken at 30 K show a drastic difference from the band dispersions at the tetragonal phase. In Figs. 2(i) and 2(j), we clearly observed three hole-like bands (α , β , γ) along k_x . The α band crosses E_F at $k_F \sim 0.04 \text{ \AA}^{-1}$, while the β and γ bands show their tops at $E - E_F \sim -20$ meV and ~ -50 meV, respectively. As summarized in Fig. 2(k), the α band has xz orbital character near the Γ point, which seems to gradually change into yz near k_F . One can thus notice that the orbital component of the α band around E_F is partly changed from yz to xz across T_s . In Geometry 2, as shown in Figs 2(l) and 2(m), we observed the α' and γ' hole bands in the left panel (s -polarization) and β' and γ' bands in the right panel (p -polarization). The α' band crosses E_F with $k_F \sim 0.10 \text{ \AA}^{-1}$, while the β' and γ' hole bands show their tops at $E - E_F \sim -20$ meV and ~ -50 meV, respectively. In Fig. 2(n), we summarized the band dispersions and orbital characters along k_y . Figures 2(k) and 2(n) show that the inequivalent band shift in xz/yz orbitals occurs around the Γ point, resulting in $E_{xz} > E_{yz}$. Considering that $E_{yz} > E_{xz}$ is realized at the M point [12], we can identify the opposite sign of the orbital polarization realized for the Γ and M

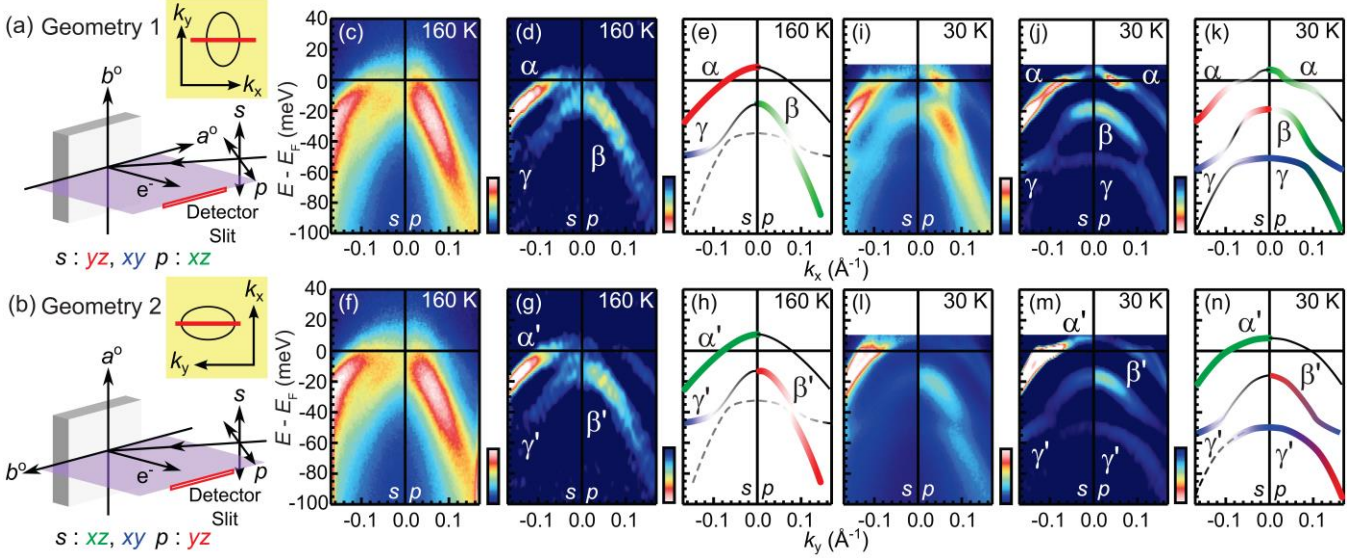


Figure 2. (a,b) Two experimental geometries for polarization-dependent laser-ARPES. In Geometry 1 (2), orthorhombic a° axis is parallel (perpendicular) to the detector slit, owing to the detwinning procedure. Purple plane represents a mirror plane of the orthorhombic lattice. Observable orbital characters are also shown for each polarization. (c,d) E - k image divided by FD function and its second E derivative detected in Geometry 1 at 160 K. The left (right) panels are E - k images obtained by s (p)-polarization. (e) Schematic band dispersions and their orbital characters. Band dispersions colored in green, red and blue are composed of xz , yz and xy orbitals, respectively. The black curves are the guides for the eyes. The broken curves represent the guides showing the band dispersions which were not clearly observed by ARPES. (f-h), The same as panel (c)-(e) taken in Geometry 2 at 160 K. (i-k), The same as panel (c)-(e) taken in Geometry 1 at 30 K. (l-n) The same as panel (c)-(e) taken in Geometry 2 at 30 K.

points. It is worth mentioning that the hole FS is mainly composed of xz orbital along k_y , and xz and yz orbitals along k_x . The k_F along k_x (k_y) is estimated to be 0.04 \AA^{-1} (0.10 \AA^{-1}) being consistent with the elliptical FS shown in Fig.1.

In order to interpret the electronic reconstruction around the Γ point, we compared the present ARPES results with the band calculations. We constructed the tight-binding model based on the DFT calculations using WANNIER90 code and WIEN2WANNIER interface. Lattice parameters used for the band calculations were taken from Ref. [26]. Then, we included the spin-orbit interaction (SOI) with $\lambda = 50 \text{ meV}$, by which the degeneracy of the xz/yz bands at the Γ point is lifted. Next, according to the previous ARPES report [27], we renormalized the band structure with the renormalization factors of ~ 3 for the xz/yz orbitals and ~ 9 for the xy orbital. Finally, realistic tight-binding model above T_s is obtained by shifting the xz/yz and xy bands as in Ref. [28]. Furthermore, in order to reproduce the orbital ordered state below T_s , we introduced the orbital polarization at the Γ point by shifting the xz (yz) band by $+7 \text{ meV}$ (-7 meV). The sign of these band shifts are opposite to those at the M point.

In the tetragonal phase, the present laser-ARPES results summarized in Fig. 3(a) are well reproduced by the band structure of the realistic tight-binding model in Fig. 3(c). The band structure is four-fold symmetric, but α , β bands are not degenerate at the Γ point, showing an energy gap of 20 meV . This gap scale is consistent with the previous

ARPES [19,20] and here we can explain it by the effect of SOI. Kink structures in the bands β and β' at $E - E_F \sim -50 \text{ meV}$ are also possibly an indication of the small gapped feature due to SOI as shown in Fig. 3(c).

In the orthorhombic phase, the calculations in Fig. 3(d) capture some important features in the present ARPES results in Fig. 3(b). Large anisotropy of the k_F is reproduced by the effect of the orbital order of $E_{xz} > E_{yz}$. The energy gap between β and γ bands is clearly observed owing to the high-energy resolution of the laser-ARPES, and considered to be a signature of the SOI. We note that the splitting energy between α and β bands at the Γ point becomes $\sim 10 \text{ meV}$ larger than that in the tetragonal phase. We thus conclude that the complex band dispersions in Fig. 3(b) are explained by the T -independent component from SOI ($\sim 20 \text{ meV}$) and T -dependent one due to the orbital order ($\sim 10 \text{ meV}$). The present result shows that in the orthorhombic phase in FeSe, the orbital polarization $f(k) = E_{yz}(k) - E_{xz}(k)$ strongly depends on k , and it becomes negative around the Γ point (-10 meV). Since the magnitude of the orbital polarization is much larger at the M point ($+50 \text{ meV}$), the relation $n_{xz} > n_{yz}$ should be satisfied similarly to other compounds.

Figures 4 (a) and (b) summarize the FSs of FeSe obtained by the detwinned ARPES above and below T_s . Schematic FSs around the Γ and M point are obtained from the ARPES data taken by $h\nu = 5.9 \text{ eV}$ and 60 eV [12], respectively. In contrast to the four-fold symmetric FS in the tetragonal phase, both the shape and the orbital component of the FSs become

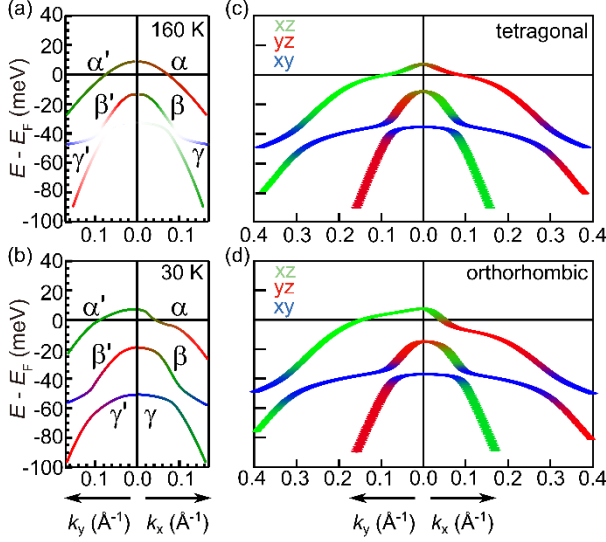


Figure 3. (a,b) Schematic band dispersions obtained by laser-ARPES at 160 K and 30 K, respectively. The left (right) panels are the results along k_y (k_x). (c,d) The band dispersions of the realistic tight-binding model including the effects of SOI and orbital order. Band dispersions colored in green, red and blue are composed xz , yz and xy orbital components, respectively.

two-fold symmetric below T_s . We can see one elliptical FS sheet around the Γ with dominantly xz orbital component. Previous ARPES on twinned FeSe reported that the two elliptical hole FSs are crossing at the Γ point. Owing to the detwinning procedure, here we clearly separated them and determined the orientation of the elliptical hole FS which is elongated along k_y .

Regarding the FS at the M point, we have reported highly anisotropic k_F in the xz and yz electron bands arising from the orbital order of $E_{yz} > E_{xz}$ [12]. Elliptical intensity around the M point in the FS mapping in Fig. 1 is consistent with this picture of anisotropic k_F . The FS corresponding to the xy band as detected in the tetragonal phase [12], on the other hand, is not clearly observed in the orthorhombic phase [depicted by the broken curves in Fig. 4(b)].

Our observation of the two elliptical FSs with different orientations at the Γ and M point is consistent with the quasiparticle interference (QPI) observed by STM/STS on FeSe [23]. As reported in ref. 23, hole (electron) band-like dispersion in the QPI image is clearly observed only along q_a (q_b) ($a > b$). Such anisotropy in the QPI images is understood by considering that the QPI is dominant between the flat portions of respective elliptical FSs at the Γ and M points.

It is also worth mentioning that the lifting of degeneracy of $E_{yz} > E_{xz}$ at the M point with its orbital polarization larger than that at the Γ point is common to several iron-based superconductors. These facts indicate that the relation in the occupied electron numbers of $n_{xz} > n_{yz}$ always holds, which might be an origin of the

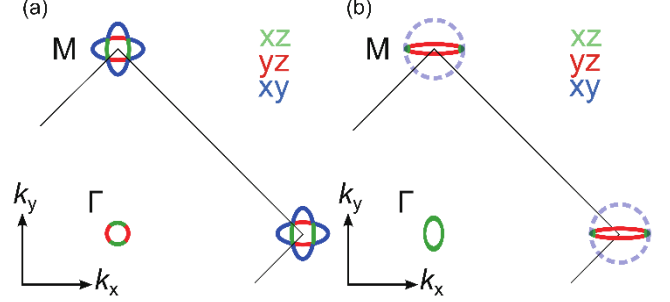


Figure 4. (a,b) Schematic FSs obtained by ARPES on detwinned FeSe in the tetragonal phase and orthorhombic phase, respectively. FSs colored by green, red and blue are composed of xz , yz and xy orbitals, respectively. Broken curve in (b) represents the electron FS sheets composed of xy orbital expected to show up, but not observed in the present ARPES. Black square represents the tetragonal Brillouin zone.

orthorhombicity. Theoretical studies suggested that the k -independent orbital polarization on the order of 10 meV resolves the magnetic frustration between $\mathbf{q} = (\pi, 0)$ and $(0, \pi)$ [16]. For FeSe, actually, strong spin fluctuations were observed for $\mathbf{q} = (\pi, 0)$ by the neutron scattering measurement [29] and its enhancement below T_s was reported by NMR measurement [30], possibly reflecting the above scenario.

However, it is puzzling that FeSe does not exhibit any AFM order despite the strongly enhanced spin fluctuation. Here we focus on the orbital polarization of $E_{xz} > E_{yz}$ around the Γ point, which has been detected only for FeSe until now. As clearly shown in this work, the k -dependent sign-inversion of orbital polarization leads to the situation that the elliptical FS at the Γ point (long-axis along k_y) is rotated by 90 degrees with respect to that at the M point (long-axis along k_x). Such electronic reconstruction makes the FS nesting condition worse. In the case of the orthorhombic/paramagnetic phase ($T_N < T < T_s$) of NaFeAs, both of the elliptical FSs at the Γ and M points are aligned with their long-axes along k_x , thus making the FS nesting condition better [11,15], which is interpreted as the driving force of the AFM order [11]. Such difference from NaFeAs may be related to the absence of the AFM order in FeSe. We can thus expect that the AFM order in FeSe is suppressed due to the imperfect FS nesting between the Γ and M points, while $(\pi, 0)$ spin fluctuations are substantially enhanced due to the magnetic frustrations resolved by the orbital ordering at T_s . Further investigations on the superconducting gap in the highly two-fold symmetric electronic structure in FeSe will give us fundamental information regarding the relation between the orbital ordering and the superconductivity in iron-based superconductors.

In conclusion, polarization-dependent ARPES study on detwinned FeSe revealed the drastic reconstruction of the FSs across T_s . The electronic structure in the orthorhombic

phase is qualitatively explained by the T -independent component from the SOI and T -dependent part due to the orbital order. We found that the xz band lifts up around the Γ point while the yz band moves up around the M point. Such momentum-dependent sign-inversion of orbital polarization modifies the FSs at the Γ and M point into elliptical shapes elongating along k_y and k_x , respectively. This modification makes the imperfect FS nesting condition, which may be related to the absence of the AFM state and electronic nematicity of orbital-origin in FeSe.

[1] Y. Kamihara, T. Watanabe, M. Hirano, and H. Hosono, *J. Am. Chem. Soc.* 130, 3296 (2008).
 [2] M. Rotter, M. Tegel, D. Johrendt, I. Schellenberg, W. Hermes, and R. Pöttgen, *Phys. Rev. B* 78, 020503 (2008).
 [3] F. Kruger, S. Kumar, J. Zaanen, and J. V. Brink, *Phys. Rev. B* 79, 054504 (2009).
 [4] W. Lv, J. Wu, and P. Phillips, *Phys. Rev. B* 80, 224506 (2009).
 [5] C. C. Lee, W.-G. Yin, and W. Ku, *Phys. Rev. Lett.* 103, 267001 (2009).
 [6] M. Yi, D. Lu et al., *Proc. Natl. Acad. Sci.* 108, 6878 (2011).
 [7] T. Shimojima et al., *Phys. Rev. B* 89, 045101 (2014).
 [8] Y. K. Kim et al., *Phys. Rev. Lett.* 111, 217001 (2013).
 [9] R. M. Fernandes et al., *Phys. Rev. Lett.* 105, 157003 (2010).
 [10] R. M. Fernandes, A. E. Böhmer, C. Meingast, and J. Schmalian, *Phys. Rev. Lett.* 111, 137001 (2013).
 [11] M. Yi et al., *New Jour. of Phys.* 14, 073019 (2012).
 [12] T. Shimojima et al., *Phys. Rev. B* 90, 121111(R) (2014).
 [13] S. Onari and H. Kontani, *Phys. Rev. Lett.* 109, 137001 (2012).
 [14] S. Nandi et al., *Phys. Rev. Lett.* 104, 057006 (2010).
 [15] Y. Zhang et al., *Phys. Rev. B* 85, 085121 (2012).
 [16] H. Kontani, T. Saito, and S. Onari, *Phys. Rev. B* 84, 024528 (2011).
 [17] A. E. Böhmer, F. Hardy, F. Eilers, D. Ernst, P. Adelman, P. Schweiss, T. Wolf, and C. Meingast, *Phys. Rev. B* 87, 180505(R) (2013).
 [18] K. Nakayama, Y. Miyata, G. N. Phan, T. Sato, Y. Tanabe, T. Urata, K. Tanigaki, and T. Takahashi, *Phys. Rev. Lett.* 113, 237001 (2014).
 [19] M. D. Watson et al., arXiv:1502.02917
 [20] P. Zhang et al., arXiv:1503.01390.
 [21] Y. Zhang et al., arXiv:1503.01556.
 [22] C.-L. Song, et al., *Science* 332 1410, (2011).
 [23] S. Kasahara et al., *Proc. Natl. Acad. Sci.* 111, 16311 (2014).
 [24] J. Omachi, K. Yoshioka, and M. Kuwata-Gonokami, *Opt. Express* 20, 23542 (2012).
 [25] S. Hüfner, *Photoelectron Spectroscopy* (Springer, Berlin, 2003).
 [26] S. Margadonna, Y. Takabayashi, M. T. McDonald, K. Kasperkiewicz, Y. Mizuguchi, Y. Takano, A. N. Fitch, E. Suard, and K. Prassides, *Chem. Commun.* 43, 5607 (2008).
 [27] J. Maletz et al., *Phys. Rev. B* 89, 220506(R) (2014).
 [28] Around the Γ point, we shift xz/yz hole bands by -0.06eV , and xy hole band by -0.08eV . Also, we shift xy/yz level and xy level by $+0.05\text{eV}$ and -0.03eV around the M points, respectively.
 [29] M. C. Rahn, R. A. Ewings, S. J. Clarke, A. T. Boothroyd, arXiv:1502.03838

[30] T. Imai, K. Ahilan, F. L. Ning, T. M. McQueen, and R. J. Cava, *Phys. Rev. Lett.* 102, 177005 (2009).